



Cause analysis and preventive measures of pipeline corrosion and leakage accident in alkylation unit

Zhenhua Tang, Zhirong Wang*, Yawei Lu, Peipei Sun

Jiangsu Key Laboratory of Hazardous Chemicals Safety and Control, College of Safety Science and Engineering, Nanjing Tech University, 21009 Nanjing, China



ARTICLE INFO

Keywords:

Corrosion leakage
Chemical composition analysis
Metallographic analysis
Corrosion products
Pipeline stress analysis

ABSTRACT

Owing to the corrosive, flammable, and explosive properties of pipeline materials in alkylation units, corrosion failure may result in leakage, fire, and explosion accidents. A bursting accident occurred in the 90° elbow of an alkylation unit pipeline. Failure analysis was performed by macroscopic analysis, metallographic analysis, chemical composition, corrosion form analysis, and corrosion product analysis. Finite element software was used to analyse the flow velocity, turbulence intensity, pressure, and wall stress distribution. The fault tree was combined with the analytic hierarchy process to realise the transformation of the structural importance-judgement factor-judgement matrix and to weight the events that may cause device corrosion failure. The results showed that uniform corrosion and stress corrosion of hydrofluoric acid occur in the pipeline and uniform corrosion is the dominant effect. Hydrofluoric acid corrosion leads to severe thinning of the pipe wall, making its strength drop below the bearing strength and rupture occurs. Quality of internal anticorrosion coating, water content of the medium and working temperature are the key factors to prevent pipeline leakage in alkylation unit.

1. Introduction

Hydrofluoric acid is used as a catalyst in the alkylbenzene plant. It is used in the form of hydrogen fluoride and hydrofluoric acid, and because of the high activity of hydrogen fluoride and hydrofluoric acid, the catalytic reaction corrodes the pipeline and equipment at the same time, threatening the safe and stable operation of the alkylbenzene unit. The current research believes that the main corrosion types of alkylation devices are uniform corrosion, hydrogen damage, stress corrosion cracking, and crevice corrosion [1]. The corrosion strength of hydrofluoric acid is affected by the concentration and temperature of hydrofluoric acid, flow rate, oxygen content, and water content [2]. Therefore, it is necessary to analyse the causes of corrosion and cracking, analyse the basic factors affecting pipeline failure, and determine the weak links of the system, which can provide a theoretical basis for the daily safety management, risk avoidance, and risk mitigation of pipelines.

Scholars have conducted research on corrosion leakage. Li et al. [3] analysed the failed test tube samples and combined the cavitation characteristics observed from the inner wall of the leaking tube and the material composition changed in the factory. They believed that cavitation was the main cause of pipeline leakage and established a simulation model to illustrate the possibility of liquid cavitation in the leakage area of the pipe. Wang et al. [4] evaluated the reliability of corroded submarine pipelines based on on-site inspection, allowable stress checks, residual strength evaluation, and remaining life estimation. Chen [5] studied the failure causes of

* Corresponding author.

E-mail address: wangzhirong@njtech.edu.cn (Z. Wang).

the X65 steel subsea pipeline in a CO₂/H₂S environment through two methods: electrochemical tests and high-temperature and high-pressure reactor simulation tests, and proposed measures to reduce the corrosion risk of the X65 steel subsea pipeline. Sun et al. [6] discussed the corrosion failure accident of a rectifying tower and obtained the corrosion failure mode of 316 L from the analysis of corrosion morphology. When the tower was operated at a low temperature (60 °C and 70 °C), the 316 L stainless steel was largely attributed to pit corrosion. At a high temperature (90 °C), the transition from pitting to stress corrosion occurs along the grain shape. Wang et al. [7–8] studied the protection of new materials against fire leakage through research on pipeline materials. Jiang et al. [9] used Fluent software to study the corrosion situation of an existing corroded pipeline, and carried out numerical simulation analysis on the influence of pipe bends, gas velocity, and pipe diameter on the centre pressure of the pipeline to evaluate its safety. Sun et al. [10] investigated the corrosion behaviour of the N80 casing during long-term use by using a corrosion reaction kettle and a weight loss method. The results show that the corrosion rate remains unchanged in the initial stage, gradually increases, and then rises sharply to 0.327 mm/a in the later stage, accompanied by an inflection point under oxygen conditions. In the absence of oxygen, the corrosion rate decreased significantly from 0.028 to 0.020 mm/a. Idris et al. [11] studied the interaction law of the radial arrangement of two or more defects. Six types of radial interaction corrosion defect arrangements were tested, and the radial limit method was used to study the influence of radial interaction. The study found that increasing the defect depth of internal and external defects would greatly reduce the failure pressure. Ben Seghier et al [12–14] evaluated the failure probability of X60 corrosion pipeline, studied the influence of corrosion defect geometry on pipeline failure, established the impact corrosion performance function. And established oil and gas based on feasibility of Support Vector Regression (SVR) and data-driven techniques. The pipeline maximum pitting corrosion prediction model and estimation frameworks. The main influencing factors for accurately predicting the maximum pitting depth of oil and gas pipelines are studied.

The research methods for the factors affecting corrosion leakage mainly include the fuzzy evaluation method, analytic hierarchy process, set pair analysis, grey correlation method, and support vector machine [15]. The analysis and calculation method of the analytic hierarchy process (AHP) is simple and easy to use. Linear algebra provides a method of mathematical expression and processing for simulation to solve problems and is widely used. Han et al. [16] combined the extension analytic hierarchy process (AHP) with the fuzzy comprehensive evaluation method and constructed a judgement matrix by replacing the specific number with the interval number, avoiding the consistency judgement of the traditional method and making the result more accurate. Xu et al. [17] introduced the analytic hierarchy process and catastrophe theory into the prediction of coal mine and gas outburst risk, in order to optimise the ranking of indicators of each layer in the catastrophe theory through the analytic hierarchy process, and improve the accuracy of the prediction model. Zhang et al. [18] proposed a complete and clear index system for the risk assessment of high-pressure gas pipelines and used the improved analytic hierarchy process (IAHP) to calculate the weight of each index and rank it. Shi et al. [19] based on the traditional and improved AHP, used Fuzzy Fault Tree Analysis (FFTA) to compare the sensitivity and importance of statistical data to determine the most critical factors leading to the accident. Guillal et al [20] revealed the influence of the mutual existence of cracks and corrosion defects on pipeline safety, and established a new probability model to predict the fracture pressure of

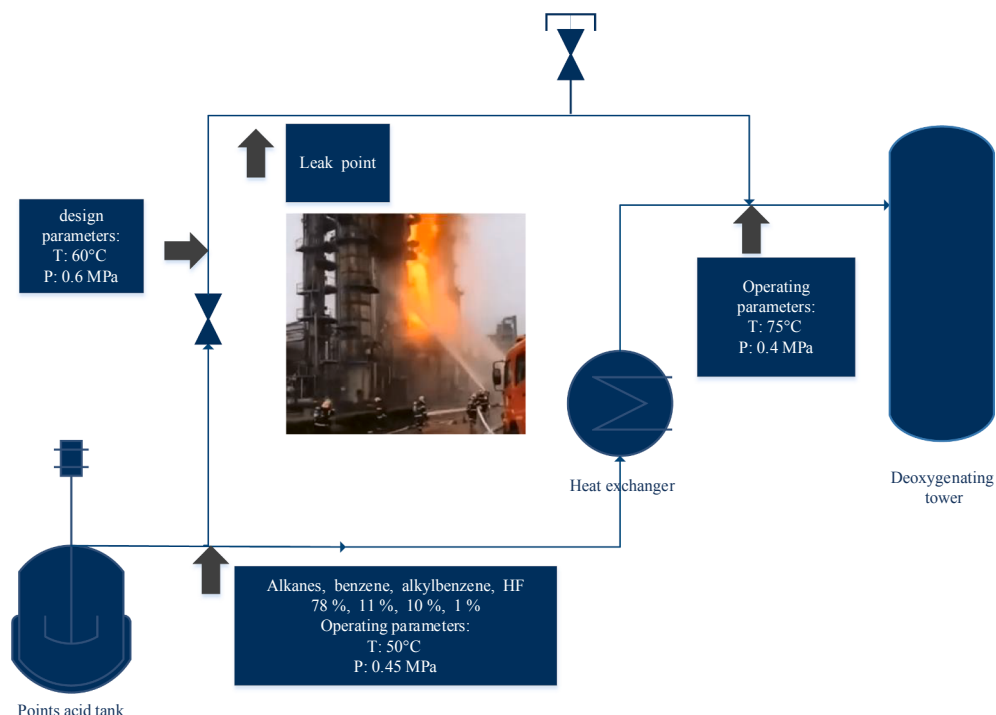


Fig. 1. Schematic diagram of the local flow at the leakage point.

the plastic collapse failure mode. Hu et al. [21] conducted a qualitative analysis of the four main factors and 14 sub-factors that caused the leakage of natural gas pipelines through the hidden danger analysis method. The study then established a layered structure model through tomographic analysis, calculated the weight of each factor, and quantitatively analysed the cause of leakage. Research on corrosion leakage mainly focuses on the corrosion leakage of sulfuric acid, H₂S, and other acidic substances on the pipeline.

There are few studies on the corrosion leakage of hydrofluoric acid, and the research on the corrosion mechanism and corrosion leakage of hydrofluoric acid is insufficient. And most scholars have only studied the physical and chemical factors that cause the failure of oil and gas pipelines. However, human factors are not considered in the failure causes, and the weights of various factors that may cause pipeline failure are not compared. Therefore, this study combines a corrosion failure accident case, through experiments and numerical simulation studies to determine the cause of pipeline failure. The fault tree model of oil and gas pipeline considering human factors is established. Use the method of combining fault tree and analytic hierarchy process to sort and analyse the basic causes of pipeline failure, and sort the importance of various causes and events. Find the weak links of risk, provide a theoretical basis for reducing the risk of pipeline failure, and propose corresponding pipeline failure prevention and control measures.

2. Incident overview

On 18 July 2020, an accident occurred at a petrochemical enterprise's alkylation unit de-benzene tower top heat exchanger tube-side cross-line pipe because of a rupture at Qixia District, Nanjing. A total of 38 fire trucks and 197 firefighters rushed to the scene to deal with the accident. The flames were extinguished one hour later, causing no casualties. The material flashed and caught fire approximately 20 s after the material was sprayed at the pipeline break. The rupture of the pipeline in the accident was located in the heat exchanger cross-line pipeline at the welding seam between the second elbow at the upper end of the horizontal pipe of the arch section of the pipeline and a straight section of the pipeline. The pipe material was 316Ti steel, pipe specification (outer diameter × wall thickness mm) Φ168 × 7.0, length was 23 m, design pressure and working pressure were 1.5 MPa and 0.6 MPa, respectively, and the working temperature was 60 °C. The medium in the pipeline was approximately 78% light wax, approximately 11% benzene, approximately 10% alkylbenzene, and approximately 1% hydrogen fluoride. The local flow at the leakage point was shown in Fig. 1.

3. Experimental and numerical simulation methods

3.1. Pipeline macro analysis and wall thickness analysis

A macroscopic analysis of the broken cross-line pipeline was performed. The residual wall thickness of the PD-T5 ultrasonic thickness gauge was used to measure the residual wall thickness of the pipe, and the reasons for the failure of the pipeline were macroscopically analysed.

3.2. Chemical composition and metallographic analysis of pipeline materials

A sample was cut from the broken section of the cross-line pipeline, sanded, polished, cleaned with absolute ethanol, and dried. The sample was then corroded with aqua regia, cleaned again with ethanol, and dried. The metallographic structure of the sample was observed using an optical microscope. An Advant XP X-ray fluorescence spectrometer was used to determine the elements of C, Si, Mn, P, S, Cr, Ni, Mo, and Ti on the inner tube of the cracked reduced exhaust gas ring.

3.3. Energy spectrum and component analysis of pipeline corrosion products

To determine the reason for pipeline corrosion cracking, it is necessary to understand the internal corrosion mechanism of pipelines and analyse the corrosion products in detail. The morphology of the corroded surface of the fractured sample was analysed using scanning electron microscopy (SEM). Energy spectrum analysis (EDS) was used to identify the chemical composition of the corrosion

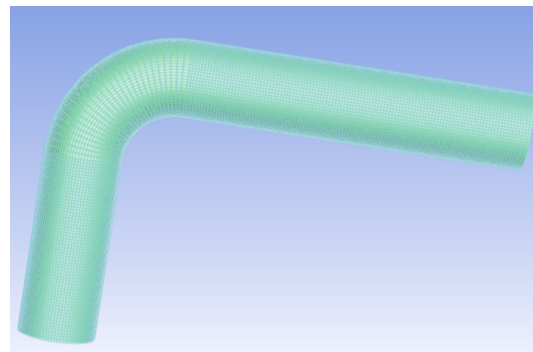


Fig. 2. Physical model of the accident pipeline.

product layer, and X-ray diffraction (XRD) was used to analyse the corrosion product composition of the fractured sample.

3.4. Pipeline fluid dynamic analysis and force finite element analysis

ANSYS Fluent software was used to simulate the accident pipeline. A three-dimensional model was established according to the structure of the pipeline, as shown in Fig. 2. A vertical section of 365 mm and a horizontal section of 676 mm were connected by a 90° elbow with a bent inner diameter of 100 mm, and the inner diameter of the pipeline was 154 mm. Computational fluid dynamics (CFD) was used to divide the mesh of the model, but since the fracture appeared in the curved section, to improve the simulation quality, mesh refinement was carried out on the elbow part. The RNGk- ϵ governing equation was used. The boundary conditions were set according to the actual working conditions of the broken pipeline. The inlet is the pressure inlet, the working pressure is 0.6 MPa, and the outlet is the flow outlet. Numerical simulations are mainly used to simulate flow characteristics such as material flow velocity, turbulent kinetic energy, pressure, and pipe wall shear stress in the actual working conditions of the pipeline in an accident.

3.5. Analysis flow chart

To facilitate the reader's understanding of the working process, analysis flow chart was established. Flowchart of pipeline failure analysis is shown in Fig. 3.

4. Results and analysis

4.1. Pipeline failure morphology and wall thickness analysis

Owing to the serious rupture of the pipeline in an accident, it is impossible to directly observe the corrosion crack location. Therefore, the 90° bend pipeline near the rupture and the pipeline fracture fragments caused by the rupture were macroscopically analysed. A cross-shaped bursting port of approximately 105 × 88 mm appeared approximately 50 mm above and before the second

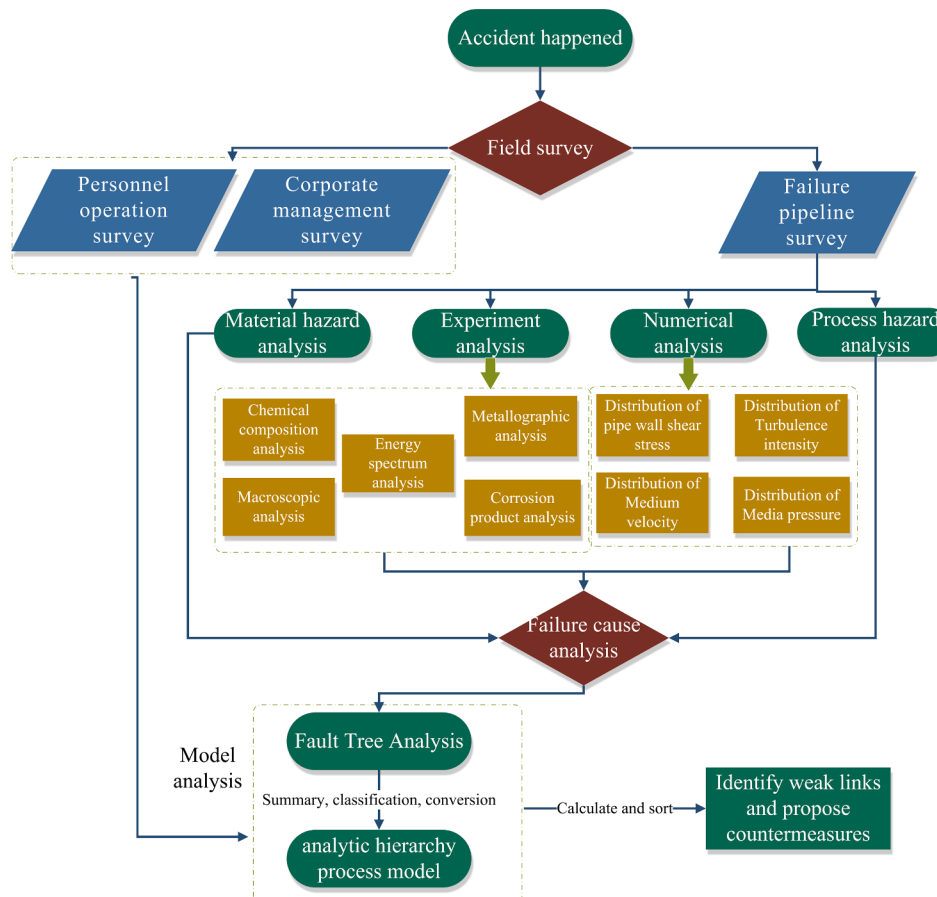


Fig. 3. Flowchart of pipeline failure analysis in this study.

elbow at the end of the pipeline, and the welding seam of the elbow was pulled apart. The blasting cross-section turns approximately 90° outward. The accident pipeline is shown in Fig. 4 (a).

The fracture was measured and analysed, as shown in Fig. 4 (b). The length of the fracture was $L = 105$ mm, the height was $H = 88$ mm, and the tear points P1 and P2 along the direction of the fracture were 25 mm and 60 mm long, respectively. Five axes, Z1, Z2, Z3, W1, and W2, were selected from the pipe end to the weld of the fracture, and the PD-T5 ultrasonic thickness measuring instrument was used to measure the wall thickness. The measurement results are presented in Table 1.

It can be observed that the thickness of the pipeline from the pipe end to the fracture weld is gradually reduced, the thickness of the fractured fragments near fracture Z1 is less than 1 mm, and the detected wall thickness near the breach is only 0.6 mm. Observation and analysis of the rupture revealed deposits inside the pipeline and a large number of volcanic bulges on the wall. As shown in Fig. 4 (c), H₂ was released when the carbon steel reacted with hydrofluoric acid, but the inside of the pipeline was volcanic. The morphology of the tiny protrusions is different from that of the hydrogen bulge, and the average impact toughness of the material is approximately 50 J, which does not decrease significantly. Therefore, the effects of hydrogen embrittlement were excluded. The thinning and blocking phenomenon at the upper end of the rupture is very serious, and serious corrosion cracks and rust marks can be observed in the thinning area of the rupture and broken fragments. This is an obvious phenomenon of stress corrosion cracking. Under the joint action of stress and a corrosive environment, the thickness of the pipeline continues to decrease, the pipeline cannot meet its bearing requirements, and cracks occur.

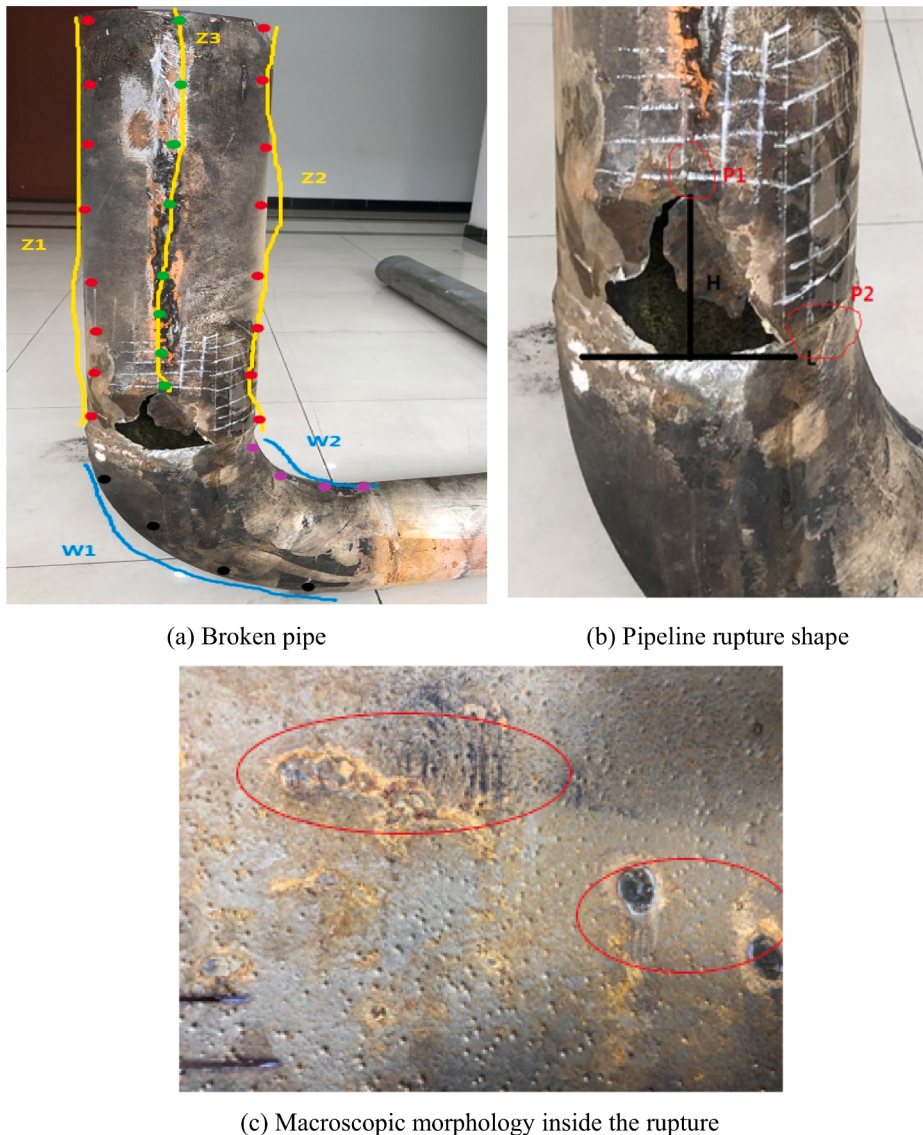


Fig. 4. Damage of accident pipeline.

Table 1

Residual wall thickness of 90° elbow pipe.

Measuring point	Normal wall thickness/mm	Z1/mm	Z2/mm	Z3/mm	W1/mm	W2/mm
1	7	1.70	1.73	5.71	4.82	4.80
2		1.12	1.30	5.10	4.93	4.94
3		1.96	1.34	1.13	5.20	4.98
4		1.43	2.02	5.27	4.94	4.90
5		1.02	1.11	3.00	—	4.86
6		1.49	1.79	1.90		5.03
7		0.99	1.56	2.52		5.05
8		0.60	1.76	2.61		—

4.2. Pipeline composition and microstructure analysis

The analysis results of the chemical element content in the broken pipe samples and unbroken pipe sample are shown in [Table 2](#). The results were compared with the standard value of 316Ti steel in GB/T 14976-2012 “Seamless Stainless Steel Pipes for Fluid Transport,” and it was found that the pipe composition meets the standard.

The results of the metallographic analysis are shown in [Fig. 5](#). By comparing [Fig. 5](#) (a) and (b), we can see the change of the metallographic structure of the broken pipeline. The figure shows that the microstructure of the sample matrix is austenite and deformation twins, and the microstructure is normal. The crack strike has both transgranular fracture and intergranular fracture. When the stress is small and the corrosive medium is weak, the stress corrosion cracks mostly extend along the grain. On the contrary, when the stress is relatively high and the corrosive medium is relatively strong, the forced corrosion cracks are usually transgranular growth [22]. There are a large number of oxides and impurity particles at the grain boundary, and the strength of the grain boundary will decrease. As a result, micro-cracks are formed at the grain boundary defects, and then extend forward along the grain boundaries with lower strength. Eventually cause fractures along the grain boundaries.

4.3. Analysis of pipeline corrosion product composition and corrosion characteristics

Samples were taken from the thinning part of the fracture pipe and the fracture fragments. The morphology of the corrosion products on the surface and the chemical composition of the corrosion product layer were analysed using SEM and EDS. The results are shown in [Figs. 6 and 7](#). The X-ray diffraction analysis results of the corrosion products on the surface of the fracture fragments are shown in [Fig. 8](#).

The microscopic morphology of the corroded surface of the pipeline sample near the breach is shown in [Fig. 6](#) (a). The figure shows that the pipe wall is covered with a thick layer of oxide, and there are cracks in the protruding part. These cracks provide a channel for the corrosive medium to penetrate into the metal surface, and the corrosive substance contacts the metal matrix through the micro-crack, leading to an increase in the corrosion rate and the possibility of local corrosion below the crack [23]. As shown in [Fig. 6](#) (b), the surface of the fracture sample mainly contains Fe, F, and O elements, and the F and O elements far exceed the F and O contents of 316Ti steel. This shows that the failure behaviour of the pipeline is closely related to the F element and its corresponding corrosion products. The microscopic morphology of the surface of the broken fragments is shown in [Fig. 7](#) (a). There are a large number of honeycomb-shaped corrosion products on the inner wall of the pipeline, indicating that the corrosion products were eroded, the compactness of the corrosion products was destroyed, and the formed product was not dense and uneven. When comparing [Fig. 6](#) (b) and 7 (b), compared with the breach, the proportion of elements such as silicon and manganese in the debris increased significantly. This shows that the medium directly reacted with the inner wall of the pipe. This led to limited ion corrosion and local pitting corrosion [24–25], and the corrosion rate was significantly faster than that of the fractured sample.

As shown in [Fig. 8](#), the corrosion products were mainly a mixture of FeF_2 and Fe_2O_3 . This indicates that, in addition to normal corrosion, the pipe was corroded by hydrofluoric acid. When the carbon steel contacts hydrofluoric acid, FeF_2 crystals are generated and H_2 is precipitated, and FeF_2 scale is formed. The escaped hydrogen provides a favourable path for ion exchange between carbon steel and corrosive media [26]. $\text{FeF}_2 \cdot 4\text{H}_2\text{O}$ was detected in the corrosion products, indicating that the water content in the medium was beyond the normal value. FeF_2 was mixed with water to form the tetrahydrate $\text{FeF}_2 \cdot 4\text{H}_2\text{O}$. The presence of water significantly affects the stability of the fluorine scale and aggravates the corrosion of hydrofluoric acid. This causes the hydrofluoric acid to continuously react with the metal wall surface, corroding the wall surface and causing the local area of the metal to continuously dissolve and thin. FeO and Fe_2O_3 were detected in the corrosion products, indicating that the oxygen in the pipeline exceeded the standard. In hydrogen fluoride gas, the presence of oxygen causes the corrosion product to be a mixture of metal oxide and metal fluoride, which is not only

Table 2

Chemical composition results of accident pipeline (W %).

Numeric type	C	Si	Mn	P	S	Cr	Ni	Mo
Broken pipe sample	0.04	0.52	0.67	0.02	0.02	16.08	10.31	2.18
Unbroken pipe sample	0.06	0.72	0.56	0.02	0.02	17.06	12.03	2.23
Standard value	≤0.08	≤1.00	≤2.00	≤0.035	≤0.03	16.00–19.00	11.00–14.00	1.80–2.50

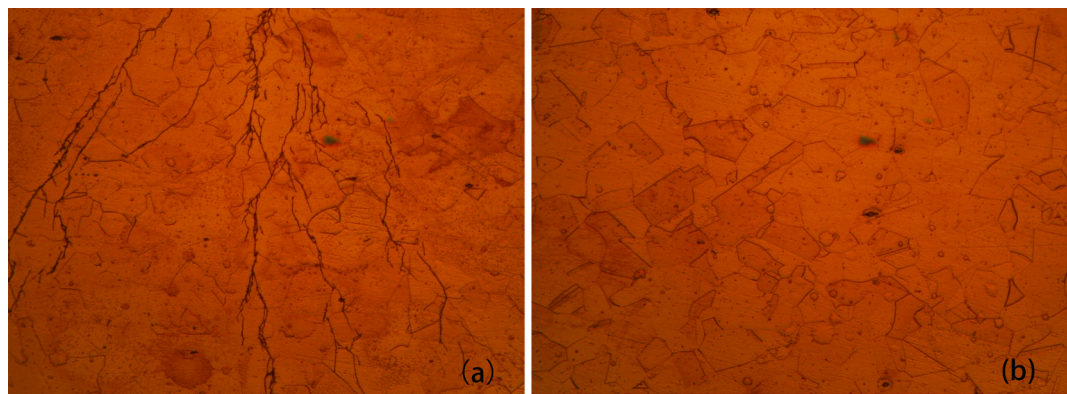


Fig. 5. Metallographic structure of the pipe sample X200 (a) broken pipe (b) Unbroken pipe.

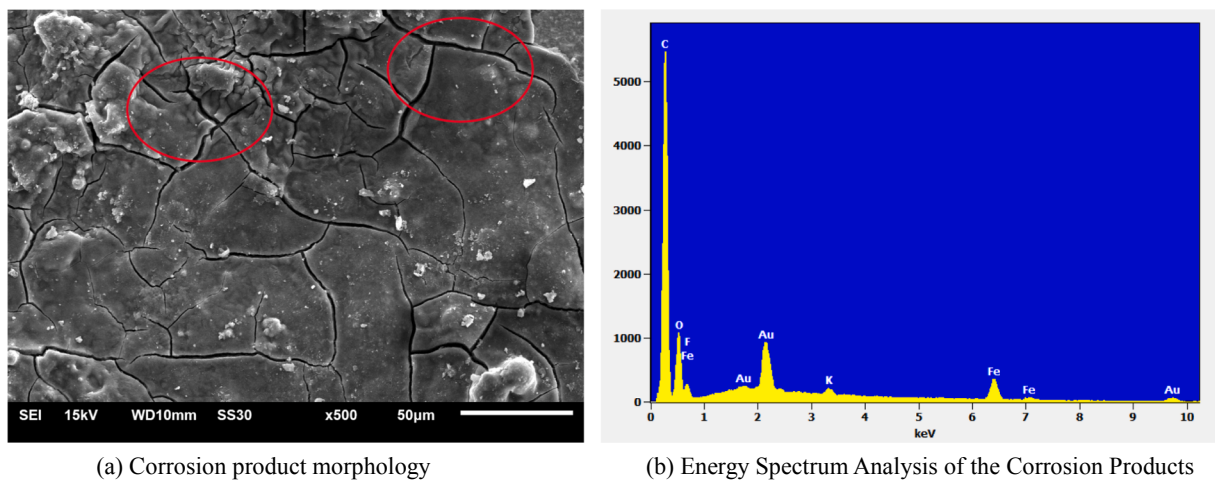


Fig. 6. SEM and EDS results near the pipe fracture.

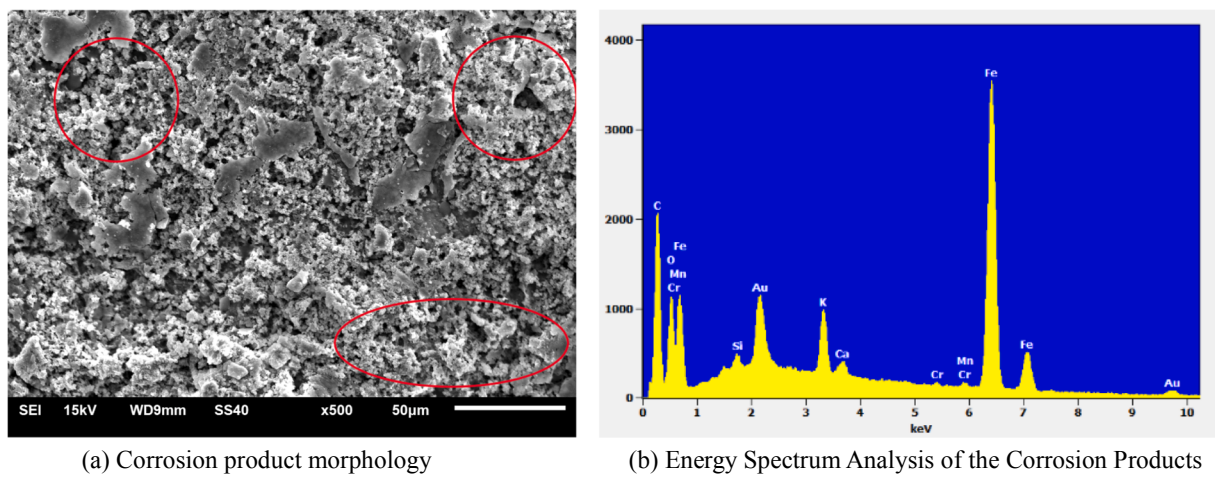


Fig. 7. SEM and EDS results of broken pipeline fragments.

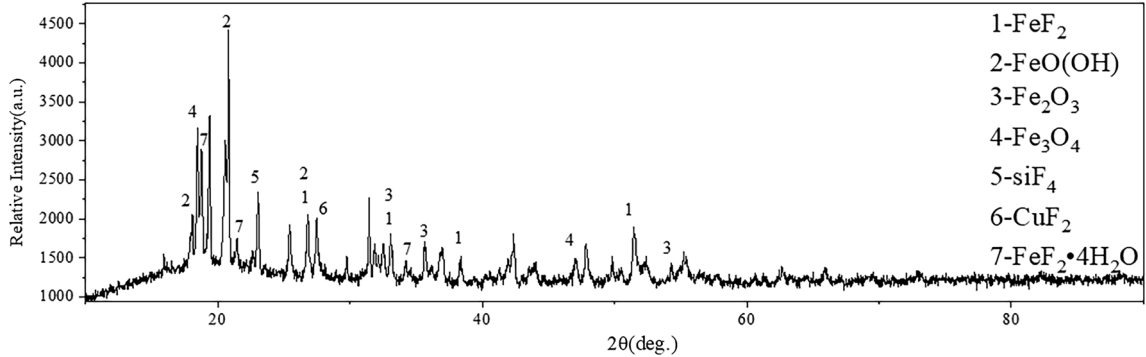


Fig. 8. XRD results of fractured fragment samples.

loose but also very brittle, and destroys the compactness of the fluoride protective film.

The above analysis shows that the dense passivation film generated by the corrosion of the accident pipeline was completely damaged, and the wall continued to react with the acid. This may have been caused by poor pigging results and poor oxygen content control of the medium during the pipeline installation process, which caused the water and oxygen in the pipeline to exceed the standard.

4.4. Pipeline material flow and force analysis

The FeF₂ scale skin will crack and fall off in the case of large turbulence changes. It is important to determine whether the pipeline medium is changed owing to the pipeline structure, which affects the passivation film and forms a corrosive environment. Therefore, through the Fluent numerical simulation, the flow characteristics of the material flow velocity, turbulence energy, pressure, and other flow characteristics in the pipeline, as well as the pipe wall shear stress during pipeline operation, were analysed.

The internal pressure distribution diagram of the pipeline is shown in Fig. 9 (c). The high-pressure position is concentrated at the outer arch of the 90° elbow. Because of inertia, after the fluid flows through the elbow, the kinetic energy is converted into static pressure, thereby increasing the pressure on the inner wall of the elbow. The turbulence intensity distribution of the medium in the accident pipeline is basically uniform, as shown in Fig. 9 (d). The turbulence intensity is greater on the inner wall of the lower side of the pipeline. Under a larger turbulence intensity, the water molecules in the medium constantly rub against the inner wall of the pipe, causing the water molecules to form local water accumulation on the inner wall of the pipe elbow. At the same time, the static pressure at the elbow further promotes the accumulation of water molecules on the inner wall of the pipe elbow [27], which provides a favourable corrosive environment for the corrosion of hydrofluoric acid. For hydrofluoric acid, even if the acid contains a small amount of water, its corrosion proceeds in accordance with the electrochemical process, resulting in metal dissolution in the pipeline and accelerated wall corrosion [28].

The velocity distribution in the pipeline is shown in Fig. 9 (b), where the velocity of the medium in the pipeline is approximately uniform, and the velocity of the contact layer between the medium and pipeline wall is small. This is because of the viscosity of the fluid itself, and the boundary layer will inevitably form on the near wall during the flow process, which further reduces the flow velocity of the medium on the pipeline wall. However, the flow velocity at the inner arch of the pipe elbow is significantly larger. Combined with the turbulence intensity distribution, the medium velocity and turbulence intensity at the inner arch are both large, which has a negative impact on the passive film formed. This is because that the passivation film is easily peeled off by the erosion of the corrosive medium. When the medium speed is too high, the corrosive medium will be constantly updated and the corrosion products will continue to move. This makes it difficult to form a passivation film on the metal surface. Especially when the medium contains solid particles, it will cause abrasion, which reduces the compactness of the passivation [29]. Thus, hydrofluoric acid continues to corrode the pipe wall, and the pipe wall becomes thinner.

The stress distribution on the pipe wall is shown in Fig. 9 (a). During normal operation of the pipeline, the internal pressure of the pipeline is 0.6 MPa. Under the influence of gravity and the 90° elbow structure, the stress on the pipeline is unevenly distributed at the elbow. It can be clearly observed that the stress distribution in the failure area of the pipeline accident was significantly greater than that in other surrounding areas. This indicates that in the failure area, the pipeline wall is subjected to a large stress. Owing to the continuous erosion and movement of the passivating film generated in the failure area, the wall corrosion of the pipeline becomes thinner. It makes the limit load of the pipeline continue to decrease. The wall thickness of the pipeline has a decisive influence on the ultimate load of the pipeline. We use the calculation formula ($P_C = \sigma_u \frac{2t}{D-t} f\left(\frac{d}{t}, \frac{L}{\sqrt{Dt}}, \frac{\beta}{\pi}\right)$) [30] of the limit load of the corroded pipeline to estimate the value of the fractured section. The least square method is used for calculation, and the formula is further expressed as:

$$P_C = \sigma_u \frac{2t}{D-t} \left[C_0 + C_1 \left(\frac{L}{\sqrt{Dt}} \right) + C_2 \left(\frac{L}{\sqrt{Dt}} \right)^2 \right] \left[G_0 + G_1 \left(\frac{\beta}{\pi} \right) + G_2 \left(\frac{\beta}{\pi} \right)^2 \right]$$

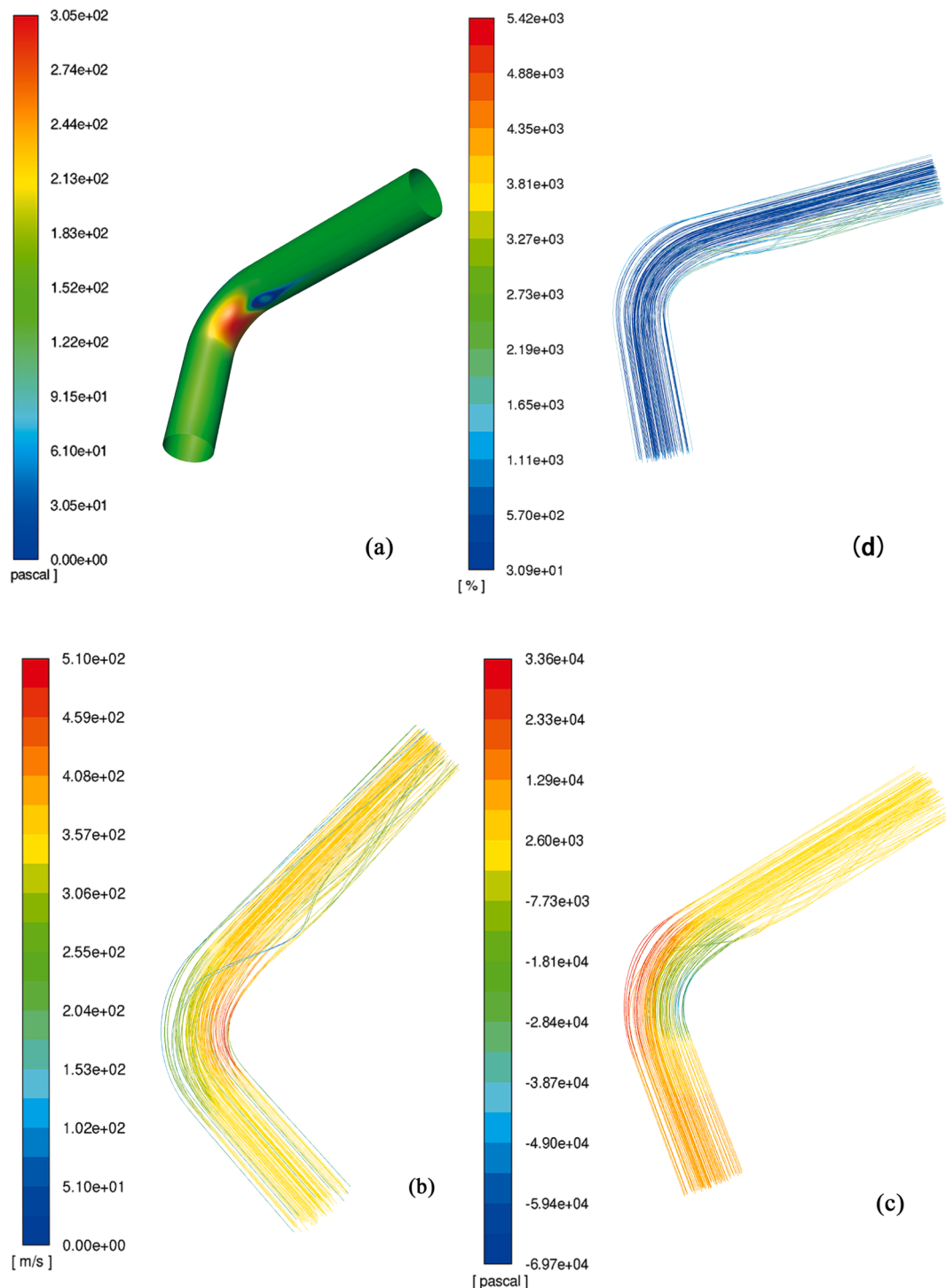


Fig. 9. Numerical analysis results of accident pipeline (a) Distribution of pipe wall shear stress (b) Distribution of medium velocity (c) Distribution of media pressure (b) Distribution of turbulence intensity.

$$c_0 = -0.8816 + 0.7942 \left(\frac{d}{t} \right) - 0.05329 \left(\frac{d}{t} \right)^2$$

$$C_1 = 0.03982 - 0.3946 \left(\frac{d}{t} \right) - 0.1901 \left(\frac{d}{t} \right)^2$$

$$C_2 = -0.004248 + 0.02983 \left(\frac{d}{t} \right) + 0.03091 \left(\frac{d}{t} \right)^2$$

$$G_0 = 1.065 - 0.2992 \left(\frac{d}{t} \right) - 0.248 \left(\frac{d}{t} \right)^2$$

$$G_1 = 0.06604 + 0.7039 \left(\frac{d}{t} \right) - 2.027 \left(\frac{d}{t} \right)^2$$

$$G_2 = -0.000185 - 1.211 \left(\frac{d}{t} \right) + 2.356 \left(\frac{d}{t} \right)^2$$

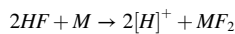
D is the outer diameter of the pipe, the pipe thickness is t , the corrosion depth is d , the corrosion length is L , β is the angle corresponding to the corrosion width, σ_u is ultimate strength. The calculation result is $p_C = 6.378 \times 10^{-6}$ MPa, From Fig. 9 (a), it can be seen that the pressure at the rupture is 2.56×10^{-4} MPa. This shows that the pipeline stress exceeds extreme pressure, causing the pipeline to rupture.

5. Discussion

5.1. Corrosion mechanism analysis

In aqueous hydrofluoric acid solutions, the corrosive effect of acid on metals and alloys is determined by the concentration of hydrogen and fluorine plasma in the acid. Hydrofluoric acid is an electrolyte solution, which is accompanied by the migration of electrons (ions) during the reaction with metals, which is a typical electrochemical corrosion [31]. The produced metal fluoride can form a passivation film to separate the pipe material from the medium, thereby weakening the corrosion of the metal material by hydrofluoric acid. The higher the temperature, the thicker the passivation film produced. However, some studies observed that when the metal temperature exceeds 65 °C, the density of the passivation film deteriorates. When the temperature exceeds 72 °C, the passivation film will fall off, or no passivation film is formed [32]. Table 3 shows the melting points and boiling points of some fluorides. It can be seen from the table that as the temperature increases, metal fluorides may volatilize and detach, which reduces the density of the passivation film. The working temperature of the pipeline in this accident is 75 °C. It shows that the pipeline in this accident was corroded by hydrofluoric acid under normal working conditions and no dense passivating film was produced inside the pipeline. The passivation corrosion behaviour was completely lost, turning into active corrosion and increasing the corrosion rate [33]. From a micro point of view, the temperature increases, and the ion movement in the solution accelerates, leading to the acceleration of corrosion. This is because, as the temperature rises, the diffusion rate of various substances in the aqueous solution accelerates and the resistance of the electrolyte aqueous solution decreases, which will accelerate the electrochemical corrosion of the electrode process of the anode and the cathode [34]. The H⁺ in hydrofluoric acid solution moves to the negative stage faster, the metal loses electrons faster, and the chemical reaction accelerates. From a macro point of view, due to the volatile hydrofluoric acid, the temperature rises, and part of the acid volatiles in the form of gas, so that the electrochemical corrosion and chemical corrosion coexist in the reaction system.

This, combined with the EDS and XRD analysis results of the pipeline medium and corrosion products, shows that the uniform corrosion and stress corrosion of hydrofluoric acid occur in the pipeline. Uniform corrosion is the predominant process, and the following reactions occur:



The anode reaction is the dissolution of metal:

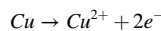
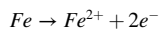
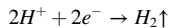


Table 3
Melting and boiling points of some fluorides.

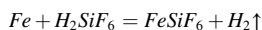
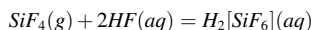
Fluorides	Melting point/°C	Boiling point/°C
NbF ₅	71	236
MoF ₆	17.5	35
WF ₆	8.3	17.5
SiF ₃	-77	-90

The cathode reaction is



The fluoride passivation film protects the pipe from direct contact with the medium and further corrosion. However, because of the influence of the pipeline structure, the state of the pipeline medium is changed, and the failure region can form a corrosion environment, preventing fluoride from being deposited on the surface. The pipe surface cannot easily form a passivation film or generates a passivation membrane that is washed off, leading to constant hydrofluoric acid corrosion of the pipe wall and pipe wall thinning. After long-term use, when the wall of the pipeline can no longer withstand the wall stress under the design pressure, the pipeline ruptures.

It is also worth noting that the corrosion products contain Si compounds (SiF_4), which are related to SiO_2 in the carbon steel [35]. These inclusions also participate in the reaction, and the reaction modes were as follows:



The SiF_4 produced by the reaction of SiO_2 with hydrofluoric acid continues to react with excess HF to produce fluorosilicic acid ($H_2[SiF_6]$), a binary strong acid that can further react with iron to release hydrogen, thus accelerating the corrosion of the pipeline.

The excess water and oxygen in the pipeline also indirectly caused pipeline failure. Even at room temperature, the electrode reaction $O_2 + 4H^+ + 4e^- \rightarrow 2H_2O$ will occur in the acidic medium of oxygen, which will accelerate the corrosion of the pipeline. Hydrofluoric acid is also significantly affected by water content. When the concentration of hydrofluoric acid is higher than 75–80%, carbon steel exhibits good corrosion resistance. This is mainly because as the concentration of hydrofluoric acid increases, the solubility of fluoride decreases, and the fluoride generated can better avoid further corrosion of the pipeline [36]. As presented in Table 4, when the concentration of hydrofluoric acid is less than 63%, the corrosion resistance of carbon steel decreases. If the water content is high, hydrofluoric acid will accelerate the corrosion of equipment, which is mainly caused by two factors. First, the concentration of hydrofluoric acid decreases, the degree of solution disintegration increases, the concentration of ions increases, and the corrosive effect of hydrofluoric acid solution on metal increases, causing the corrosion of the hydrofluoric acid solution to metals. The second factor is the presence of water, which leads to the decomposition of metal fluoride, thus destroying the passivation film and increasing the corrosion rate.

The equipment involved in the accident used 316Ti steel in the main pipelines. We also inspected other pipelines adjacent to the accident pipeline. However, there was no local corrosion phenomenon similar to that of the failed pipeline. According to our analysis, the reasons for this corrosion are as follows.

- (1) There is a stagnant protection layer adjacent to the pipe wall, and turbulence rarely occurs, which protects the fluoride passivation film from destruction and protects the pipe. The failed pipeline forms a vortex at the 90° elbow. The material behind the elbow is relatively stable without a large flow, and hydrogen fluoride is prone to stratification in the pipeline.
- (2) During the installation of the failed pipeline, the pigging results were poor and the oxygen content of the medium was poorly controlled, which caused the water and oxygen in the pipeline to exceed the standard. This provides a favourable corrosive environment for the corrosion of hydrofluoric acid and aggravates the corrosion of the pipeline.
- (3) When the operating temperature of the accident pipeline is approximately 75 °C, the passivation film produced has poor compactness, and the film will fall off, or even not form at all.
- (4) Because of the high turbulence intensity, the water molecules in the medium often rub against the inner wall of the pipe, leading to the aggregation of water molecules, and along the inner wall of the pipe, local water molecules further aggregate on the inner wall of the elbow. The static pressure at the elbow cut pipe further promotes the accumulation of water molecules on the inner wall of the pipe elbow, which intensifies the corrosion.

Ferric fluoride produced when hydrogen fluoride meets carbon steel has a certain protective effect on the corrosion of steel, but temperature rise or turbulence destroys the protective layer and aggravates corrosion. According to the operating conditions, and owing to the material stratification, there may be trace hydrofluoric acid and gas phase material generated by the pressure difference.

Table 4
Corrosion rate of carbon steel in hydrofluoric acid at 20 °C.

Hydrofluoric acid concentration (wt.%)	Corrosion rate/(mm·a ⁻¹)
60	2.30
61	2.10
62	1.50
63	0.22
64	0.05
65	0.05
67.5	0.05
69.9	0.07

Therefore, local phase change corrosion is formed on the upper part of the cross-line pipeline, and pipeline rupture occurs under the operating pressure condition.

In summary, the reasons for accident pipeline rupture and leakage are as follows:

Under the corrosion action of hydrogen fluoride and hydrofluoric acid, the wall thickness of the pipeline was severely reduced. The pipe therefore cannot meet its bearing strength capacity and fails.

5.2. Cause analysis of corrosion leakage

5.2.1. Fault tree analysis of corrosion leakage

Through the investigation of the accident site, the company's management inspection, and the inspection records, and combined with the test results, some events that may cause pipeline corrosion and leakage accidents of the alkylation unit are listed individually. The fault tree is drawn based on the complexity, diversity, uncertainty, and other factors of alkylation pipeline failure. Choice: "corrosion failure" is the top event T. Corrosion perforation and corrosion cracking are the direct causes of T, which are taken as secondary top events for further analysis. Finally, an accident tree is drawn according to the logic, as shown in Fig. 10. Table 5 shows the meaning of each basic event, corresponding to 20 basic events in total.

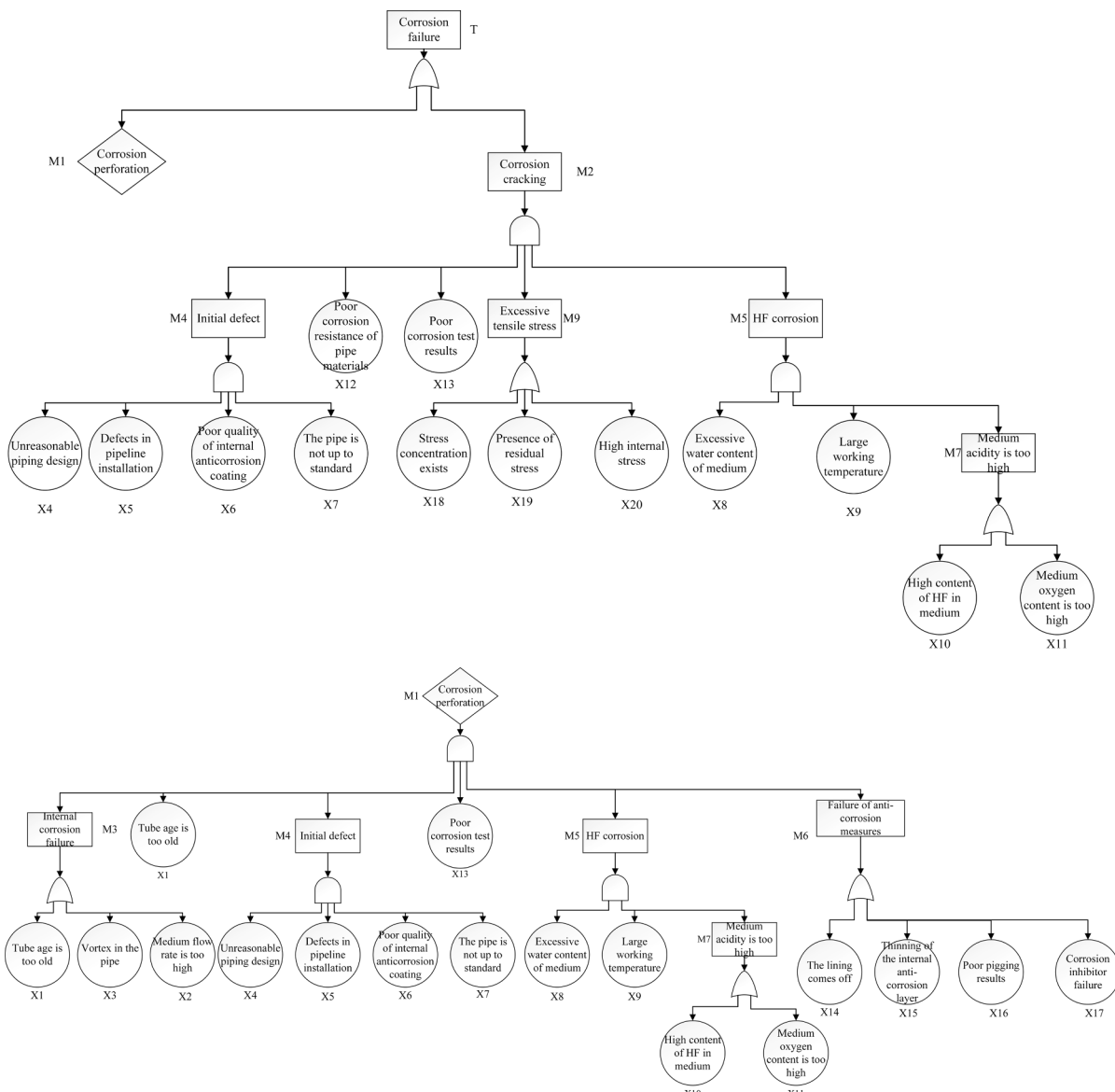


Fig. 10. Corrosion leakage accident tree of the alkylation unit.

Table 5

Meaning of the basic events of the fault tree.

Serial number	Basic event	Serial number	Basic event
X1	Tube age is too old	X11	Medium oxygen content is too high
X2	Medium flow rate is too high	X12	Poor corrosion resistance of pipe materials
X3	Vortex in the pipe	X13	Poor corrosion test results
X4	Unreasonable piping design	X14	The lining comes off
X5	Defects in pipeline installation	X15	Thinning of the internal anti-corrosion layer
X6	Poor quality of internal anticorrosion coating	X16	Poor pigging results
X7	The pipe is not up to standard	X17	Corrosion inhibitor failure
X8	Excessive water content of medium	X18	Stress concentration exists
X9	Large working temperature	X19	Presence of residual stress
X10	High content of HF in medium	X20	High internal stress

5.2.2. Analysis of the structural importance of corrosion factors

Because the analytic hierarchy process can determine the weight of each risk factor for pipeline accidents, it can determine the maintenance, repair, and inspection measures during pipeline operation in a targeted manner. These measures can be taken purposefully, according to the importance of the accident factor measures, to reduce pipeline risks [37]. Therefore, according to the fault tree model in Fig. 10, the basic events are summarised, classified, and described, and then transformed into factors in each indicator layer in the analytic hierarchy process. Then, through further classification and description, the criterion layer is determined to be corrosion, pipeline materials and equipment defects, and misoperations. A final established AHP model is shown in Table 6.

The weight of each indicator layer in the analytic hierarchy process reflects the degree of influence on the target layer. In the accident tree, the structural importance is based on the model without considering the probability of a basic event. Therefore, the degree of importance of the roles of structural importance and weight is consistent. When constructing the judgement matrix, there is a greater subjective tendency to judge the important relationship between the two factors while comparing the two factors with each other. Thus, we take the least common multiple LCM of the structural importance of each basic event to calculate the judgement factor X_i ($X_i = I\Phi(i) \cdot \text{LCM}$, $I\Phi(i)$ is the structural importance of each event). The judgement factors of basic events are used to construct the pairwise judgement matrix. Because each criterion layer corresponds to a certain number of index layer factors, the judgement factor of the criterion layer can be represented by the sum of the judgement factors of the index layer. The judgement factors of each event calculated according to their structural importance are shown in Table 7.

According to the results in Table 7, the judgement factors of criterion layer corrosion, pipeline material and equipment defects, and misoperation are 713, 639, and 328, respectively, which are used as criterion layer judgement factors. The corresponding criterion layer and index layer judgement matrices and comparisons are established, respectively, as matrix A , B_1 , B_2 , and B_3 .

$$\text{criterion layer } A = \begin{pmatrix} 1 & 3 & 7 \\ 1/3 & 1 & 5 \\ 1/7 & 1/5 & 1 \end{pmatrix}$$

$$\text{Index layer } B_3 = \begin{pmatrix} 1 & 1 & 9 \\ 1 & 1 & 9 \\ 1/9 & 1/9 & 1 \end{pmatrix} B_1 = \begin{pmatrix} 1 & 1/3 & 1/3 & 1/3 & 3 & 3 & 7 \\ 3 & 1 & 1 & 1 & 7 & 7 & 9 \\ 3 & 1 & 1 & 1 & 7 & 7 & 9 \\ 1/3 & 1/7 & 1/7 & 1/7 & 1 & 1 & 2 \\ 1/3 & 1/7 & 1/7 & 1/7 & 1 & 1 & 2 \\ 1/7 & 1/9 & 1/9 & 1/9 & 1/2 & 1/2 & 1 \end{pmatrix} B_2 = \begin{pmatrix} 1 & 1 & 3 & 9 & 9 & 8 & 8 & 8 \\ 1 & 1 & 3 & 9 & 9 & 8 & 8 & 8 \\ 1/3 & 1/3 & 1 & 7 & 7 & 6 & 6 & 6 \\ 1/9 & 1/9 & 1/7 & 1 & 1 & 1/2 & 1/2 & 1/2 \\ 1/9 & 1/9 & 1/7 & 1 & 1 & 1/2 & 1/2 & 1/2 \\ 1/8 & 1/8 & 1/6 & 2 & 2 & 1 & 1 & 1 \\ 1/8 & 1/8 & 1/6 & 2 & 2 & 1 & 1 & 1 \\ 1/8 & 1/8 & 1/6 & 2 & 2 & 1 & 1 & 1 \end{pmatrix}$$

A consistency test of the above judgement matrices was performed, and the results are as follows:

matrix	the largest eigenvalue	CI ratios	RI ratios	CR ratios	consistency examination results
A	3.066	0.033	0.520	0.063	pass
B_1	7.079	0.013	1.360	0.010	pass
B_2	8.201	0.029	1.410	0.020	pass
B_3	3.00	0.000	0.520	0.000	pass

It can be observed that the CR ratios of the constructed matrix are all less than 0.1, which indicates that the constructed matrix has passed the consistency test. The distribution of these weights can be considered reasonable. After calculation, the weight vectors are $A = (1.930, 0.849, 0.221)$, $B_1 = (0.766, 1.841, 1.841, 1.841, 0.272, 0.272, 0.166)$, $B_2 = (2.536, 2.536, 1.472, 0.212, 0.212, 0.343, 0.343)$, and $B_3 = (1.421, 1.421, 0.158)$. Then, the weight of the index layer to the target layer from the weight vector of each layer is calculated to perform a total ranking of the levels. The weight of each risk and factor of a pipeline accident can be determined. The calculation results and final weight ranking results are listed in Table 8.

Table 6

Hierarchical analysis of pipeline corrosion leakage in the alkylation unit.

Target layer	criterion layer	Index layer
Corrosion and leakage of alkylation unit pipeline	corrosion	X1 Tube age is too old X6 Poor quality of internal anticorrosion coating X8 Excessive water content of medium X9 Large working temperature X10 High content of HF in medium X11 Medium oxygen content is too high X15 Thinning of the internal anti-corrosion layer X4 Unreasonable piping design X7 The pipe is not up to standard X12 Poor corrosion resistance of pipe materials X14 The lining comes off X17 Corrosion inhibitor failure X18 Stress concentration exists X19 Presence of residual stress X20 High internal stress X5 Defects in pipeline installation X13 Poor corrosion test results X16 Poor pigging results
	Pipeline material and equipment defects	
	Misoperation	

Table 7

Structural importance and judgement factors of basic events.

Basic event	structure importance	Judgement factor	Basic event	structure importance	Judgement factor
X1	3/4	105	X12	7/10	98
X4	1	140	X13	1	140
X5	1	140	X14	12/35	48
X6	1	140	X15	12/35	48
X7	1	140	X16	12/35	48
X8	1	140	X17	12/35	48
X9	1	140	X18	11/28	55
X10	1/2	70	X19	11/28	55
X11	1/2	70	X20	11/28	55

Table 8

Weight order of basic events.

Factor	Weights	Factor	Weights
X6	3.55313	X15	0.32038
X8	3.55313	X5	0.314041
X9	3.55313	X13	0.314041
X4	2.153064	X18	0.291207
X7	2.153064	X19	0.291207
X1	1.47838	X20	0.291207
X12	1.249728	X14	0.179988
X10	0.52496	X17	0.179988
X11	0.52496	X16	0.034918

As presented in Table 8, the first three events with the highest weight are the poor quality of the internal anti-corrosion layer, high water content of the medium, and high working temperature, which are the key links in preventing the leakage of the alkylation unit pipeline.

6. Conclusions and recommendations

Through a systematic in-depth analysis of pipeline corrosion and leakage, the main conclusions are as follows:

- (1) Uniform corrosion and stress corrosion of hydrofluoric acid occurred inside the pipeline in which uniform corrosion played a dominant role.
- (2) The pipe structure leads to the aggregation of water molecules in the failure area, and the pipe inner wall forms local water aggregation on the inner wall of the elbow, which provides conditions for the corrosion of hydrofluoric acid.
- (3) The pipeline wall is severely thinned because of the corrosion of hydrogen fluoride and hydrofluoric acid, reducing its strength to below load-bearing strength and resulting in failure.

- (4) The fault tree model of alkylation pipeline failure was established. The fault tree was combined with the analytic hierarchy method to realise the transformation of the structural importance-judgement factor-judgement matrix, which made the evaluation result more objective.
- (5) Evaluation result shows that the quality of the internal anti-corrosion layer, water content of the medium, and control of the working temperature are the key factors that prevent leakage of the alkylation unit pipeline.

According to the influencing factors of corrosion leakage, the following safety measures are recommended:

- (1) Control the water content of hydrofluoric acid in the alkylation unit. The water content of the alkylation unit should be strictly controlled within 0.3–0.5%. Controlling the dry benzene water content, reducing the water content in the circulating acid, and reducing the dehydration burden of the hydrofluoric acid regeneration tower can form a virtuous cycle.
- (2) Control the reaction temperature of the alkylation unit. The corrosion resistance of carbon steel decreases with an increase in the reaction temperature. The reaction temperature of the alkylation unit should be maintained below 65 °C.
- (3) The internal corrosion layer uses a better composite corrosion inhibitor. For hydrofluoric acid, the formulated composite corrosion inhibitor can form a stable adsorption film on the surface of carbon steel through physical and chemical adsorption. Meanwhile, the protective film formed by physical adsorption can make it difficult for H⁺ in the solution to approach carbon steel. On the surface, the cathode discharge effect is blocked, thereby reducing the corrosion rate of hydrofluoric acid to carbon steel.
- (4) Control the oxygen content of the alkylation units. Purification of the alkylation unit requires multiple purges and replacement of equipment and pipelines with nitrogen. Improving the quality of nitrogen, especially by reducing the water content and oxygen content in nitrogen, will delay the corrosion of equipment and shorten the contact time between the inside of the equipment and air. The moisture in air condenses on the surface of the equipment and decomposes the metal fluoride. In addition, the presence of oxygen further destroys the compactness of the fluoride protective film and accelerates corrosion.
- (5) Control the flow rate of the alkylation unit medium. When the flow rate is high enough, the corrosive medium is constantly updated, the corrosion products are constantly moved, and the passivation film on the metal surface is difficult to form, especially when the medium contains solid particles, which causes abrasion.

There are still some shortcomings in this paper, such as not considering the impact of man-made damage and natural disaster damage on pipeline failure. The established evaluation system is only for alkylation pipeline failure accidents. Next, we will collate the oil and gas pipeline failure accidents published in domestic and foreign literature in the past 15 years, compare various factors in the index layer, and establish and verify the method applicable to the whole oil and gas pipeline.

Declaration of Competing Interest

The authors declare that they have no known competing financial interests or personal relationships that could have appeared to influence the work reported in this paper.

Acknowledgements

The authors are grateful for National project funding for Key R & D programs under Grant No. 2018YFC0808500, National Natural Science Foundation of China under Grant No. 52074159, Key R & D programs(Social Development) in Jiangsu Province under Grant No. BE2020710, Key National Natural Science Foundation of China under Grant No. 51834007, Key Natural Science Foundation in Jiangsu Province under Grant No. 18KJA620003, and Jiangsu Project Plan for Outstanding Talents Team in Six Research Fields(TD-XNYQC-002).

References

- [1] J.P. Wu, L. Zhang, Corrosion and control of HF alkylation unit. The 6th Academic Conference of the Department of Chemical Engineering, Metallurgy and Materials Engineering, Chinese Academy of Engineering. Chinese Academy of Engineering, 2007.
- [2] M. Roche, C. Grenet, M. Richez, Troubleshooting corrosion problems in hf alkylation units - sciencedirect, *Corrosion Refineries* (2007) 64–72.
- [3] W.M. Li, Y.R. Lv, Z.W. Sun, W. Yu, Cause analysis of corrosion leakage in convection section of ethylene cracking furnace, *Eng. Fail. Anal.* 111 (2020), 104488.
- [4] Z.J. Wang, Z.H. Wen, J.P. Zhou, L. Geng, B.F. An, W.D. Chen, Submarine transportation pipeline safety assessment system and its application, *Corrosion Protection* 33 (10) (2012) 903–907.
- [5] R.Q. Chen, Applicability of X65 steel subsea pipeline in CO₂/H₂S corrosive environment, *Corrosion Protection* 33 (05) (2012) 371–374.
- [6] P. Sun, Z. Wang, Y. Lu, S. Shen, R. Yang, A. Xue, T. Parker, J. Wang, Q. Wang, Analysis of the corrosion failure of a semiconductor polycrystalline distillation column, *Process Saf. Environ. Prot.* 135 (2020) 244–256.
- [7] J.L. Wang, C. Ma, X.W. Mu, W. Cai, L.X. Liu, X. Zhou, W.Z. Hu, Y. Hu, Construction of multifunctional MoSe₂ hybrid towards the simultaneous improvements in fire safety and mechanical property of polymer, *J. Hazard. Mater.* 352 (2018) 36–46.
- [8] J.L. Wang, D. Zhang, Y. Zhang, W. Cai, C.X. Yao, Y. Hu, W.Z. Hu, Construction of multifunctional boron nitride nanosheet towards reducing toxic volatiles (CO and HCN) generation and fire hazard of thermoplastic polyurethane, *J. Hazard. Mater.* 362 (2019) 482–494.
- [9] H.F. Jang, L.P. Gao, J. Yang, Evaluation leakage safety and numerical simulation of existing corroded natural gas pipeline. *Shanxi Architecture* 47(04) (2021) 104–105+108.
- [10] X. Sun, R.L. Nan, B.Z. Shu, H. Wang, L.J. Zhu, L.H. Han, Corrosion behavior for casing in producing well with water injection technology during long-term service, *Mater. Sci. Forum* 5930 (2020) 1168–1173.

- [11] N.N. Idris, Z. Mustaffa, M.E.A. Ben Seghier, N.T. Trung, Burst capacity and development of interaction rules for pipelines considering radial interacting corrosion defects, *Eng. Fail. Anal.* 121 (2021), 105124.
- [12] M.E.A. Ben Seghier, B. Keshtegar, J.A. Correia, G. Lesiuk, A.M. De Jesus, Reliability analysis based on hybrid algorithm of M5 model tree and Monte Carlo simulation for corroded pipelines: Case of study X60 Steel grade pipes, *Eng. Fail. Anal.* 97 (2019) 793–803.
- [13] M.E.A. Ben Seghier, B. Keshtegar, K.F. Tee, T. Zayed, R. Abbassi, N.T. Trung, Prediction of maximum pitting corrosion depth in oil and gas pipelines, *Eng. Fail. Anal.* 112 (2020), 104505.
- [14] M.E.A. Ben Seghier, B. Keshtegar, M. Taleb-Berrouane, R. Abbassi, N.T. Trung, Advanced intelligence frameworks for predicting maximum pitting corrosion depth in oil and gas pipelines, *Process Saf. Environ. Prot.* 147 (2021) 818–833.
- [15] J.P. Wang, X.L. Wang, L.G. Zhou, L. Shao, Pipeline risk factor weighting method based on subjective-objective integrated weight, *Oil Gas Storage Transport.* 38 (07) (2019) 745–750.
- [16] L.H. Han, J.W. Liu, Q.L. Yin, Green building green degree evaluation based on fuzzy extension analytic hierarchy process, *Value Eng.* 38 (12) (2019) 127–129.
- [17] B.Y. Xu, X.J. Li, AHP-catastrophe theory in coal mines and application research series in gas outburst risk prediction, *Mining Technol.* 19 (03) (2019) 64–66.
- [18] Y. Zhang, S.R. Lv, W.Q. Wang, Risk analysis of high pressure gas pipeline leakage based on bow-tie model and IAHP, *IOP Conference Series: Earth Environmental Science* 461 (1) (2020) 12079.
- [19] L. Shi, S. Jian, X. Kui, Fuzzy fault tree assessment based on improved AHP for fire and explosion accidents for steel oil storage tanks, *J. Hazard. Mater.* 278 (2014) 529–538.
- [20] A. Guillal, M.E.A. Ben Seghier, A. Nourddine, J.A. Correia, Z. Bt Mustaffa, N.T. Trung, Probabilistic investigation on the reliability assessment of mid- and high-strength pipelines under corrosion and fracture conditions, *Eng. Fail. Anal.* 118 (2020), 104891.
- [21] H.R. Hu, B.K. Zhu, J. Guo, Natural gas pipeline leakage analysis based on advance risk analysis and analytic hierarchy process, *IOP Conference Series: Earth Environmental Science* 565 (2020) 12019.
- [22] M.A. Mohaddi-Bonab, Effects of different parameters on initiation and propagation of stress corrosion cracks in pipeline steels: a review, *Metals* 9 (5) (2019) 590, <https://doi.org/10.3390/met9050590>.
- [23] S.G. Xu, S.J. Huang, D.G. Guo, Y.J. Zhao, M.D. Song, Failure analysis of a carbon steel pipeline exposed to wet hydrogen sulfide environment, *Eng. Fail. Anal.* 71 (2017) 1–10.
- [24] B. Liu, X.L. Wei, W.L. Wang, J.F. Lu, J. Ding, Corrosion behavior of Ni-based alloys in molten NaCl-CaCl₂-MgCl₂ eutectic salt for concentrating solar power, *Sol. Energy Mater. Sol. Cells* 170 (2017) 77–86.
- [25] S.X. Shen, Z.R. Wang, J.C. Jiang, X.Y. Cao, P.P. Sun, Y.W. Lu, R.R. Yang, Synergistic Effect of the Total Acid Number, S, Cl, and H₂O on the Corrosion of AISI 1020 in Acidic Environments, *ACS Omega* 5 (2020) 20311–20320.
- [26] C. Liu, R.I. Revilla, D.W. Zhang, Z.Y. Liu, A. Lutz, F. Zhang, T.L. Zhao, H.C. Ma, X.G. Li, H. Terryn, Role of Al₂O₃ inclusions on the localized corrosion of Q460NH weathering steel in marine environment, *Corros. Sci.* 138 (2018) 96–104.
- [27] J.D. Wang, X.Q. Huang, W.L. Qi, C.Y. Zhang, Y. Zhao, Y. Dai, T. Zhang, F.H. Wang, Corrosion failure analysis of the 45-degree elbow in a natural gas gathering pipeline by experimental and numerical simulation, *Eng. Fail. Anal.* 118 (2020), 104889.
- [28] B. Wei, Corrosion mechanism and protective measures of chemical machinery, *Chem. Eng. Des. Commun.* 3 (04) (2017) 149–157.
- [29] S. Feng, W.S. Qu, H.F. Wang, L. Jin, C.X. Zhang, Safety evaluation methods comparison of submarine pipelines with corrosion defects, *Petro-chemical Equipment* 49 (01) (2020) 10–16.
- [30] C.L. Su, X. Li, J. Zhou, Impacts of axial corrosion width on ultimate internal pressure load of pipeline, *Oil Gas Storage Transport.* 33 (07) (2014) 723–728.
- [31] Schweitzer, *Corrosion and Corrosion Protection Handbook*, CRC Press, 2017.
- [32] G.C. Hong, Corrosion and protective measures of hydrofluoric acid rotary reactor, *Petro-chemical Equipment.* (01) (2008) 54–56.
- [33] Q.M. Lu, *Corrosion and protection in the petroleum industry*, Chemical Industry Press, 2001.
- [34] M. Masoumi, H.F.G. Abreu, L.F.G. Herculano, J.M. Pardal, S.S.M. Tavares, M.J.G. Silva, EBSD study of early fractured phenomena in a 350 grade maraging steel elbows exposed to hydrofluoric acid, *Eng. Fail. Anal.* 104 (2019) 379–387.
- [35] T.V. Shibaeva, V.K. Laurinavichyute, G.A. Tsirlina, A.M. Arsenkin, K.V. Grigorovich, The effect of microstructure and non-metallic inclusions on corrosion behavior of low carbon steel in chloride containing solutions, *Corros. Sci.* 80 (2014) 299–308.
- [36] X. Chen, L. Yang, H.L. Dai, S.W. Shi, Exploring factors controlling pre-corrosion fatigue of 316L austenitic stainless steel in hydrofluoric acid, *Eng. Fail. Anal.* 113 (2020), 104556.
- [37] J. Fang, F.Y. Partovi, Criteria determination of analytic hierarchy process using a topic model, *Expert Syst. Appl.* 169 (2020), 114306.